The PVD neuron has male-specific structure and mating function in *C. elegans*

Yael Iosilevskii[1] and Benjamin Podbilewicz[1,#]

[1]Department of Biology, Technion- Israel Institute of Technology, Haifa 32000, Israel

[#]Correspondence should be addressed to B.P. (podbilew@technion.ac.il).

Keywords: PVD neuron; Sexual dimorphism; Male behavior; Dendrite arborization; *C. elegans;* SAX-7/L1CAM; Menorin complex

Summary

Neurons display unique shapes and establish intricate networks, which may differ between sexes. In complex organisms, studying sex differences in structure and function of individual neurons is difficult. The nematode *Caenorhabditis elegans* hermaphrodites and males present an exceptional model for studying neuronal morphogenesis in a simple, sexually-dimorphic system. We focus on the polymodal sensory bilateral neuron pair PVD, which forms a complex but stereotypic dendritic tree composed of multiple subunits that resemble candelabra. PVD was previously studied in hermaphrodites, but not in males. We find here that during larval development, male PVDs extend a similar architecture to the hermaphrodite utilizing a sexually-shared patterning mechanism. In early adulthood, however, male PVD develops a unique extension into the copulatory tail structure. This sexually-dimorphic arborization is absent in mutant backgrounds which perturb the sex-shared PVD guidance complex. SAX-7/L1CAM, a hypodermal component of this complex, shows a male-specific expression pattern which precedes PVD extension. Further, our results reveal that genetically altered arborization or ablation of the PVD result in male mating behavioral defects, particularly as males turn around the hermaphrodite. These results uncover an adult-stage sexual dimorphism of dendritic branching and uncover a new function for PVD in male sexual behavior.

Introduction

Neurons grow distinctive morphologies and form sophisticated networks [1–5]. These networks often show sexual dimorphism, with different connectivity and distribution between the sexes [3,4,6–9]. In humans, many neurological disorders are more common in one sex (*e.g.* attention deficit hyperactivity disorder (ADHD), autism spectrum disorder, and Parkinson's disease are more prevalent in men, while major depression, eating disorders and dementia are more common in women, reviewed in [10]). While altered neuron shape, in particular dendritic spines, has been associated with some of these conditions [11–13], it remains difficult to establish the role of particular dendritic morphologies with animal behavior, and whether they relate to sexual dimorphism at a single-neuron level.

The nematode *Caenorhabditis elegans* has been widely used as a model organism for studying neuron morphology [2,4,14], connectivity [2,3,15], plasticity [16–21] and activity [15,22,23]. While the majority of the population are hermaphrodites, loss of one X chromosome yields males [24–26], which are sexually dimorphic in anatomy [27], neuronal connectivity [4], and behavior [24,28,29]. Both the hermaphrodite and the male's compact nervous system consists of diverse neuron types and morphologies, which enable a variety of behaviors including directed movement (towards and away from odors, temperature ranges [30,31], salt [32,33] and carbon dioxide concentrations [34]) and escape (from chemical contact [35], gentle or noxious touch [36–39], ultraviolet light [40] and directed sound [41]). Uniquely, each neuron's identity and the connectome linking them together have been established [2–4]. A small population of neurons in *C. elegans* that presents highly arborized dendrites has served as a robust system for analyzing neuron patterning and development [42,43], among them the neuron pair PVD [44–47].

Each of two PVD neurons (left and right) assumes its structure during the final three out of four larval stages of a hermaphrodite's development (L2-L4) [44,45] (Figure 1A). PVD is a polymodal sensory neuron which senses noxious touch [44,48,49], temperature drops [50], sound vibration[41] and body position [51,52]. Its characteristic branching, forming repetitive subunits which resemble candelabra ('menorahs' [44]), develops through actin-mediated growth [53–55]. The hermaphrodite PVD morphogenesis is guided by the Menorin multipartite complex, in which transmembrane receptors from the PVD, notably the leucine-rich repeat transmembrane domain (LRR-TM) protein DMA-1 [56], bind hypodermal (epidermal) and muscle-expressed guidance cues, notably SAX-7/L1CAM and MNR-1/Menorin [53,57,58]. Its initial branching is governed in part by a LIM homeobox domain transcription factor, MEC-3 [36,37,45,59,60]. In addition to the Menorin patterning

complex, multiple pathways maintain neuron tiling, self-avoidance, and excessive branching pruning events, among them UNC-6/Netrin [55,61], KPC-1/Furin [62–64] and the cell-cell fusogen EFF-1 [44,65]. With age and following dendritic injury, PVD loses its characteristic form and develops excessive 'ectopic' branches, which extend beyond the young-adult form [19,66,67] (Figure 1B).

Sexually dimorphic behavior in *C. elegans* can arise from altered expression of sensory channels [39,68], variation in synaptic connectivity and strength [38,69] and different gene expression networks [29,70], some of which may already be active prior to sexual maturation [71]. However, to our knowledge, specific and robust differences in complex dendritic arborization between hermaphrodite and male *C. elegans* have not been characterized. We focus on PVD, and ask whether its complex arbor has any sexually dimorphic features. Here, we show PVD develops a post-larval, male-specific element of dendrite morphology, which extends into the specialized rays of the male tail, previously thought to contain only two neurons (RnA and RnB) [27]. This post-larval morphogenesis is consistent with a sexually dimorphic distribution of the hypodermal patterning cue SAX-7/L1CAM, acting within the sexually-shared Menorin patterning complex previously characterized in the hermaphrodite [54,56–58,63,64,72–74]. We further show that in addition to its sensory functions in hermaphrodites, PVD is required for precise male mating behavior, revealing an additional sex-specific role. Our results uncover sexual dimorphism in PVD morphogenesis and function, which also open directions for studying adult-onset directed dendritic branching.

Results

PVD morphology is sexually dimorphic

While much is known about hermaphrodite PVD dendritic tree morphogenesis [44,45], it remains unclear whether males share the same structure, patterning mechanism, and function. To determine the wildtype (WT) PVD structure of the male, we imaged animals either from stocks continuously maintained with males [75] or carrying a *him-5(e1490)* background mutation which increases the male percentage [28]. We found that male PVD develops candelabra-shaped dendritic units, similar to the hermaphrodite (Figure 1C-F). Four branching orders are maintained; the male primary branch is compressed medially compared with the hermaphrodite (Videos S1 and S2). Branch density relative to body length is higher in the males (Figure 1G), with altered distribution of ectopic branching (Figure 1H). Interestingly, we noted that in early adulthood male PVD further extends into the sexually dimorphic tail rays (Figure 1F). The male rays support a specialized tail fan (Figure 1I) required for mating [76,77], and each of the nine bilateral rays was previously shown to contain only two neurons, RnA and RnB [27,78]. This unexpected finding encouraged us to explore this novel pattern of male PVD morphology further.

In order to determine the temporal component for PVD dendritic entry into the tail rays, we analyzed WT animals at different time points. We found that PVD does not enter the rays as they first form in the fourth larval stage (L4); rather, PVD ray extension takes place around the final L4-to-adult molting (Figure 1E,F). As the animals progress into the first days of adulthood, the PVD gradually establishes dendrite extensions into the rays in a laterally-stochastic fashion (Figure 1J), also demonstrated by flow of photoconvertible Kaede protein from the cell body to the rays (Figure S1). Lateral tiling is maintained as in the hermaphrodite [44,79], with PVDL and PVDR (left and right, respectively) extending dendrites into the respective left or right sides of the tail with no overlap (Video S3).

Hermaphrodite-characterized PVD patterning mutants show similar male phenotypes

To determine whether PVD patterning mechanisms are sexually shared, we imaged *eff-1(ok1021)*; *mec-3(e1338), sax-7(dz156), mnr-1(dz175)* and *dma-1(tm5159)* mutant male animals carrying a PVD-expressed marker and found that these backgrounds show similar PVD morphogenesis defects to hermaphrodites [45,57,58,60] (Figure 2B-F). These results reveal that the roles of *mec-3* and *eff-1* in PVD branching are sex-shared, and that the Menorin guidance

pathway participates in male PVD morphogenesis. We note that as part of these defects, PVD also fails to extend into the tail rays in these backgrounds (Figure 2I).

Ray width is the determining factor for PVD elaboration within a ray

The extension of PVD branches into the male rays during early adulthood (Figure 2I) presents a unique model to explore the contribution of surrounding anatomy on dendritic shaping. To determine the effect of ray anatomy on subsequent PVD extension, we studied *mab-20(bx61)*, which presents an increased percentage of joined ('fused') rays [80], in which two or more rays are displaced and join to share an epidermal sheath [78]. We hypothesized that ray width is the determining factor for PVD tendency to branch or turn within a ray. Indeed, our analysis of joined rays revealed they often had a single PVD dendritic process, which may turn or branch further within the ray (Figure 2G, Figure S2B-E). In the WT, ray 6 is naturally wider compared with the rest [80], and shows the same phenomenon (Figure S2A,E). Although PVD morphology alters within wider rays, the extension into the ray itself is not dependent on its width; *mab-20(bx61)* ray-associated PVD entry remains comparable with WT (Figure 2I), suggesting that ray placement has little effect on subsequent PVD extension, but wider rays allow a single PVD dendrite to further branch and turn within it (Figure S2E).

PVD dendrite entry into tail rays is affected by tail morphology and the fusogen eff-1

While ray width seems to determine PVD branching within each ray, ray placement (as altered in the *mab-20* context) showed little effect. We therefore turned to mutants which show more severe structural tail defects. To determine how overall tail morphology and PVD dendrite extension interact, we examined mutants of the epithelial fusogen *eff-1* which governs the correct formation of the syncytial hypodermis [81]. Mutants of *eff-1* show deformed tails, with a small fan and short rays [81] . In hermaphrodites, PVD is characteristically hyperbranched, extending multiple ectopic branches [44], a phenotype we note is also true for males (Figure 2B, Figure S2H). In males, however, this hyperbranching does not confer enhanced branching into the tail rays (Figure 2I). Rather, loss of *eff-1* inhibits PVD extension into the tail rays, in a dosage-dependent manner, as established by comparison of *eff-1(hy21ts)* temperature-sensitive allele at restrictive and permissive temperatures (Figure S2F-I). While impaired, *eff-1* PVD ray extension rises with animal age (Figure S2J) as in the WT, indicating the neuron remains dynamic while the surrounding ray deformities inhibit its morphogenesis.

Ray neurons RnBs are independent of PVD dendrites

To date, two neurons innervating the male tail rays were identified, named RnA and RnB (each numbered n=1-9 and bilateral; R1A(R/L), R2A(R/L) etc.) [27]. To study whether ray 'resident' neurons such as RnBs and PVD branches are interdependent during tail morphogenesis, we constructed a strain co-expressing distinct fluorescent reporter proteins for RnB (GFP) and PVD (mCherry). We found that in L4 animals, as the rays are projecting, RnB is already present within each ray, while PVD is absent (Figure 3A-C, n=54 rays observed, Video S4). In adult animals, PVD was partially associated with RnB within the lumbar and pre-anal ganglions as well as the rays, which contain RnB but may or may not contain PVD (Figure 3D; n=92 adult rays observed). We conclude that male PVD and RnB follow different patterning mechanisms, and their extension is temporally separated.

sax-7 patterning precedes PVD dendrite entry into the male tail rays

Noting the arborization defects seen in Menorin complex mutant backgrounds also inhibit PVD extension into the tail rays (Figure 2I), we wondered whether known PVD patterning cues of the Menorin adhesion complex, notably the axonal guidance molecule SAX-7/L1CAM [57,58,62,65,73,74,82–84], are present in the developing rays. We imaged males carrying an integrated low-copy number fosmid-based reporter for *sax-7* translation [82,84] and found that during L4, a *sax-7*p::*sax-7*::GFP signal is visible within the nascent rays (Figure 3E-F). This patterning precedes PVD extension (Figures 3C,1E). In the adult, PVD signal follows over the tail ray *sax-7::*GFP pattern, which is prominent in all the rays (as also shown by [85]), (Figure 3G-J, n=113 rays observed). Thus, in male adults, *sax-7* expression in the ray hypodermis appears to guide the entry of PVD branches into the tail (Figure 3I). This conclusion is supported by the *sax-7* loss-of-function mutant phenotype, which results in truncated posterior PVD (Figure 2D). These results suggest a model whereby the sexually dimorphic aspect of PVD morphogenesis utilizes components of the established intercellular guidance complex in the hermaphrodite [57,58,62,63,65,73,74,82–84], however with a male-specific distribution and at a heterochronic post-larval developmental stage.

PVD initiates dendritic branching into the rays prior to the onset of male mating behavior

Male mating in *C. elegans* is a complex multi-step process, performed by a male animal upon encountering a hermaphrodite [77]. Its execution relies on male-specific neurons and neural circuits [3] which guide chemosensory sexual attraction [68,86] and mechanosensation [77,87,88] as well

as on sexually-dimorphic anatomy, in particular the male tail [27,77,88]. Once a male has located a hermaphrodite using chemosensory cues, the male circles around it tail-first until the tail makes contact with the hermaphrodite's vulva [77]. The male then inserts its two copulatory spicules and ejaculates sperm into the hermaphrodite's uterus [77]. PVD is not open to the external environment or known to play any chemosensory role, leading us to focus on steps in male mating behavior which may involve mechanosensation [37,44,49] and proprioception [51,52]. We chose to analyze three behavioral steps: 1) Contact recognition, which is the initial reversal in response to tail contact with a hermaphrodite; 2) precise turning around the head or tail of the hermaphrodite during backwards movement to maintain scanning for the vulva; and 3) stopping at the vulva (Figure 4A) [77].

Having observed that WT PVD enters into the tail rays, we sought to find whether this correlates with proficient mating ability. L4 males, where PVD has not yet entered into the tail rays (Figure 2I), are also lacking a functional sensory tail fan structure [27]. This meant the earliest age we could use for behavioral analysis was young adults that have just molted, where PVD is already detected in some rays (Figure 2I). At this stage, many of the males analyzed displayed poor contact recognition of hermaphrodites (Figure S3A, YA, Video S5). 24h later, the same animals (kept in isolation) showed an improvement in mating turning and vulva recognition, comparable with same-aged virgin males (Figure S3B,C, Video S5). Age therefore correlates with increased PVD entry into the tail rays (Figure S3D) and simultaneously contributes to mating performance and turning ability (Figure S3E), but precise turning does not require a high percentage of rays to contain PVD (Figure S3F). Perhaps unsurprisingly, very young males may not perform mating behavior at all (9/45 showed no contact recognition response; only 5/33 successfully mate versus 5/6 one-day adult controls). Since young males' mating behavior shows high variability at a time where PVD has already extended into the tail rays (Figures 2I, S3A-C), we conclude that PVD male-specific branching precedes the onset of the adult mating behavior repertoire. Following this observation, we used one-day adult males which show robust mating behavior in the WT, in order to compare backgrounds with altered PVD morphology.

PVD affects male mating behavior

Some mutations which affect PVD morphology have been associated with reduced PVD-mediated nociceptive response in hermaphrodites, for example in *mec-3* [37,60] and *eff-1* [44] animals. As mentioned above, *eff-1* mutants are uninformative for mating assays, since they present male tail abnormalities (Figure S2F-H) [81]. On the contrary, *mec-3(e1338), sax-7(dz156),*

mnr-1(dz175) and *dma-1(tm5159)* show normal tail morphology (Figure 2C-F) and were assayed for male mating. Impaired mating behavior was observed in all four genetic backgrounds (Figure S4), particularly and consistently in turning (Figure S4E-H). Combined, these results pointed to a potential role for PVD in a male-specific behavior, affected at least in part by its dendritic morphology.

As PVD may not be the only neuron affected in the mutant backgrounds tested (*e.g. mec-3* affects gentle-touch neurons and the head nociceptor FLP [36,37], *sax-7* affects VD and DD motor neuron axon path [89] and the male-specific PHC [85]), we asked whether PVD is specifically required for male mating behavior. For this purpose we analyzed a strain where PVD is genetically ablated [51] by specific expression of *deg-3(u662)* dominant-negative mutation which induces neuron degeneration (in neurons which express DEG-3 nicotinic acetylcholine receptor subunit [90]). In the hermaphrodite, PVD genetic ablation results in altered crawling motion [51]. We found that in males with PVD genetic ablation, mating behavior was impaired in all three steps of hermaphrodite recognition, turning and vulva stopping (Figure 4), with turning being the most notable (Figure 4C). Together with the prominent behavior impairment seen in the above four mutant backgrounds, these results suggest the PVD plays a novel role in adult male mating behavior, in particular during steps which require proprioception.

Discussion

Sexual dimorphism in anatomy and behavior is prevalent across the animal kingdom [10,91,92], in plants [93] and some algae [94–97]. In humans, several neurological conditions show a clear sexual bias [10]. While studies can detect differences in male and female model animals of depression[98], Alzheimer's disease [99] and possibly attention deficit and hyperactivity disorder (ADHD) [100], the role of individual neuron morphology in sexually dimorphic behavior and disease remains elusive[101]. Mating behavior represents a robust sexually-dimorphic behavioral system for studying underlying neuroanatomy-driven differences using simpler organisms [6,102–104].

The PVD dendritic tree is elaborate, distinct, and extends the majority of the worm's length. Our analysis revealed that while hermaphrodite PVD largely maintains its late L4 morphology in early adulthood [57,58], male PVD undergoes further extension in the posterior region into the male-specific tail rays in early adulthood (Figure 1F, Figure 2I). This observation provides a unique post-larval branching model, perhaps more akin to dendrite maintenance and aging than

to morphogenesis (Figure 5). This represents a morphogenesis mechanism distinct from that of a 'resident' ray neuron, RnB (Figure 3A-D). This plastic development extends from the hermaphrodite guidance complex adopting a sexually dimorphic distribution, through ray-specific SAX-7 expression (Figure 3E-J). This dependence of PVD on a hypodermal patterning component, alongside the tendency of its dendritic processes to turn and branch within 'fused' rays or the wider ray 6 in the WT (Figure S2A-E), suggests PVD projects in relation to the ray hypodermis. Association of PVD and RnB at the pre-anal ganglion region (Figure 3D) conforms with connectome studies, which suggest that synapses form between PVD and RnB (Figure S5) [4].

In addition to developing a male-specific dendritic morphology, it is possible that sexually-dimorphic connectivity (Figure S5) also occurs during early adulthood, in parallel with an improvement in mating behavior (Figure S3A-C). While PVD-PVC connectivity was followed in the hermaphrodite [105], it is important to note that much of our knowledge of PVD synaptic partners relies on a male electron microscopy series reconstruction, for which comparable hermaphrodite reconstructions are as yet missing [2,4].

As a complex process, male mating relies on multiple parameters to perform correctly: long and short-distance chemosensation [106,107], mechanosensation [87,108], proprioception [77], and consideration of environmental factors such as starvation and starvation cues [86,109,110]. Alongside 'dedicated' mating-related ray neurons such as RnA [88], we show that PVD is important for contact response, male turning around the hermaphrodite and vulva recognition (Figure 4). Recent studies recording global neuron activity in mating males confirm PVV, which synapses onto PVD [4], is robustly activated during turning, while PVZ is active during vulva recognition [108,111]. Other male-specific neurons which synapse onto PVD (Figure S5) [4] either activate during other steps (SPV in sperm release), are inconclusive (R1B) or were not recorded (R6B and PVD itself) [108,111]. While existing connectome data supports a connection between PVD and mating-related neurons, the single PVV-PVD synapse noted [4] may be too weak to form a distinct sensory circuit (Figure S5). As such, it is plausible that PVD functions during male mating as a proprioceptor, rather than as part of a male-specific mating neuronal circuit.

While we cannot rule out the possibility that PVD branching in certain ray combinations is important for turning behavior, as was demonstrated by global ablations of all or some ray neurons [77,88], this is difficult to ascertain in WT adults (Figure S3G). Temporally, PVD extension into a male's tail rays occurs prior to the appearance of robust mating behavior (Figure S3D-F).

When studying hermaphrodite mutant alleles with impaired PVD morphogenesis, previous studies noted some behavioral effects, such as reduced nociceptive response in *dma-1(tm5159)* mutant animals [52] and altered crawling pattern in PVD misrouting brought about by *sax-7* removal in the adjacent ALA interneuron [53]. Importantly, *sax-7* mutant males were previously shown to have defects in contact response as well as vulva location efficiency [85]. Our results provide evidence for additional male-specific behavioral defects (Figure S4) in animals with impaired PVD morphology (Figure 2C-F). Recent studies demonstrated local calcium transients in quaternary and tertiary branches of the PVD [52,112], which can be elicited by stretch and deformation of candelabra dendritic units as the animal moves [52]. It is interesting to note that all mutant backgrounds examined here show defects in menorah morphology, which could eliminate this proprioceptive response (see Figure 2C-F), in line with this PVD sensory function [51,52].

PVD branching into the tail rays precedes a striking change in male mate-seeking behavior and mating capacity from L4 to adulthood. While PVD activity and morphology are not the sole contributor of male sexual behavior [77,88,111], PVD may be modulated as part of a male-specific, adult-specific, learning process. Complete and specific ablation of the PVD results in male behavior defects (Figure 4), which are consistent with PVD's role as a proprioceptor [51,52,113], and extend the role of PVD for fine motor skills specifically required in males.

Our results uncover a previously uncharacterized role for PVD in male mating behavior, and reveal a sexually dimorphic instance of post-larval specific branching into the male tail rays, which seems integral to the early adult dendritic arbor. Further work is required to directly establish the mechanisms regulating PVD ray entry, and to elucidate the direct function of this dendritic morphology together with body candelabra in proprioception and male behavior.

Acknowledgements

We are grateful to Yehuda Salzberg, Hagar Setty and Meital Oren for strains (EB1564, EB1271, EB1653, DA509, MOS81) and valuable advice regarding mating experiments, to Kang Shen for TV15911 and TV15916, and to Millet Treinin for MF288. We thank Scott Emmons, David Hall and Hannes Bülow for their valuable comments regarding PVD connectivity. Son Le Tho for preliminary analyses of sexual dimorphism in PVD branching. Shay Stern, Dan Cassel, Menachem Katz and Meital Oren for critically reading the manuscript. Some strains were obtained from the *Caenorhabditis* Genetics Center (CGC) which is funded by the NIH Office of

Research Infrastructure Programs (P40 OD01440). Research in our lab has received funding from the Israel Science Foundation (2462/18, 2327/19, 178/20 and 1575/21 to B.P.) and Dirección General de Asuntos del Personal Academico, Programa de Estancias de Investigación (PREI), UNAM, Mexico City (B.P.).

Author contributions

Y.I. conceived and conducted experiments, collected and analyzed data and wrote the manuscript. B.P. conceived experiments, secured funding, oversaw, managed and coordinated research activities, provided review, commentary, and revision of the manuscript.

Declaration of interests

The authors declare no competing interests.

Supplemental information

Document S1:

Figures S1–S5 and Table S1

STAR Methods

Movie legends

Supplemental References

Video S1. Hermaphrodite traced PVD neuron rotation, related to Figure 1B

Video S2. Male traced PVD neuron rotation, related to Figure 1F

Video S3. Traced PVDL and PVDR, related to Figure 1J

Video S4. Male PVD and RnB traced in the L4, related to Figure 3C

Video S5. Mating of WT young adult to adult transition, related to Figure 4

References

1. Ghysen, A., Dambly-Chaudière, C., Aceves, E., Jan, L.-Y., and Jan, Y.-N. (1986). Sensory neurons and peripheral pathways in Drosophila embryos. Rouxs. Arch. Dev. Biol. *195*, 281–289.

2. White, J.G., Southgate, E., Thomson, J.N., and Brenner, S. (1986). The structure of the nervous system of the nematode Caenorhabditis elegans. Philos. Trans. R. Soc. Lond. B Biol. Sci. *314*, 1–340.

3. Jarrell, T.A., Wang, Y., Bloniarz, A.E., Brittin, C.A., Xu, M., Thomson, J.N., Albertson, D.G., Hall, D.H., and Emmons, S.W. (2012). The connectome of a decision-making neural

network. Science *337*, 437–444.

4. Cook, S.J., Jarrell, T.A., Brittin, C.A., Wang, Y., Bloniarz, A.E., Yakovlev, M.A., Nguyen, K.C.Q., Tang, L.T.H., Bayer, E.A., Duerr, J.S., et al. (2019). Whole-animal connectomes of both Caenorhabditis elegans sexes. Nature *571*, 63–71.

5. Merritt, D.J., and Whitington, P.M. (1995). Central projections of sensory neurons in the Drosophila embryo correlate with sensory modality, soma position, and proneural gene function. J. Neurosci. *15*, 1755–1767.

6. Kimura, K.-I., Ote, M., Tazawa, T., and Yamamoto, D. (2005). Fruitless specifies sexually dimorphic neural circuitry in the Drosophila brain. Nature *438*, 229–233.

7. Ciofi, P., Leroy, D., and Tramu, G. (2006). Sexual dimorphism in the organization of the rat hypothalamic infundibular area. Neuroscience *141*, 1731–1745.

8. Cachero, S., Ostrovsky, A.D., Jai, Y.Y., and Dickson, B.J. (2010). Sexual dimorphism in the fly brain. Curr. Biol.

9. Sacher, J., Neumann, J., and Okon-Singer, H. (2013). Sexual dimorphism in the human brain: evidence from neuroimaging. Magnetic resonance.

10. Palanza, P., and Parmigiani, S. (2017). How does sex matter? Behavior, stress and animal models of neurobehavioral disorders. Neurosci. Biobehav. Rev. *76*, 134–143.

11. Kulkarni, V.A., and Firestein, B.L. (2012). The dendritic tree and brain disorders. Mol. Cell. Neurosci. *50*, 10–20.

12. Kasai, H., Ziv, N.E., Okazaki, H., Yagishita, S., and Toyoizumi, T. (2021). Spine dynamics in the brain, mental disorders and artificial neural networks. Nat. Rev. Neurosci. *22*, 407–422.

13. Forrest, M.P., Parnell, E., and Penzes, P. (2018). Dendritic structural plasticity and neuropsychiatric disease. Nat. Rev. Neurosci. *19*, 215–234.

14. Chalfie, M., and Thomson, J.N. (1979). Organization of neuronal microtubules in the nematode Caenorhabditis elegans. J. Cell Biol. 10.1083/jcb.82.1.278.

15. Chalfie, M., Sulston, J.E., White, J.G., Southgate, E., Thomson, J.N., and Brenner, S. (1985). The neural circuit for touch sensitivity in Caenorhabditis elegans. J. Neurosci. *5*, 956–964.

16. Cohn, J.A., Cebul, E.R., Valperga, G., Brose, L., de Bono, M., Heiman, M.G., and Pierce, J.T. (2020). Long-term activity drives dendritic branch elaboration of a C. elegans sensory neuron. Dev. Biol. *461*, 66–74.

17. Giordano-Santini, R., Kaulich, E., Galbraith, K.M., Ritchie, F.K., Wang, W., Li, Z., and Hilliard, M.A. (2020). Fusogen-mediated neuron−neuron fusion disrupts neural circuit connectivity and alters animal behavior. Proc. Natl. Acad. Sci. U. S. A. *117*, 23054–23065.

18. Giordano-Santini, R., Linton, C., and Hilliard, M.A. (2016). Cell-cell fusion in the nervous system: Alternative mechanisms of development, injury, and repair. Semin. Cell Dev. Biol. *60*, 146–154.

19. Oren-Suissa, M., Gattegno, T., Kravtsov, V., and Podbilewicz, B. (2017). Extrinsic repair of injured dendrites as a paradigm for regeneration by fusion in Caenorhabditis elegans. Genetics *206*, 215–230.

20. Schroeder, N.E., Androwski, R.J., Rashid, A., Lee, H., Lee, J., and Barr, M.M. (2013). Dauer-specific dendrite arborization in C. elegans is regulated by KPC-1/furin. Curr. Biol. *23*, 1527–1535.

21. Wicks, S.R., and Rankin, C.H. (1996). The integration of antagonistic reflexes revealed by laser ablation of identified neurons determines habituation kinetics of the Caenorhabditis elegans tap withdrawal response. Journal of Comparative Physiology - A Sensory, Neural, and Behavioral Physiology. 10.1007/BF00216131.

22. Bargmann, C.I. (2006). Chemosensation in C. elegans. Preprint, 10.1895/wormbook.1.123.1 10.1895/wormbook.1.123.1.

23. Yemini, E., Lin, A., Nejatbakhsh, A., Varol, E., Sun, R., Mena, G.E., Samuel, A.D.T., Paninski, L., Venkatachalam, V., and Hobert, O. (2021). NeuroPAL: A Multicolor Atlas for Whole-Brain Neuronal Identification in C. elegans. Cell *184*, 272–288.e11.

24. Brenner, S. (1974). The genetics of Caenorhabditis elegans. Genetics *77*, 71–94.

25. Hodgkin, J.A., and Brenner, S. (1977). Mutations causing transformation of sexual phenotype in the nematode Caenorhabditis elegans. Genetics *86*, 275–287.

26. Nigon, V., and Dougherty, E.C. (1949). Reproductive patterns and attempts at reciprocal crossing of Rhabditis elegans Maupas, 1900, and Rhabditis briggsae Dougherty and Nigon, 1949 (Nematoda: Rhabditidae). J. Exp. Zool. *112*, 485–503.

27. Sulston, J.E., Albertson, D.G., and Thomson, J.N. (1980). The Caenorhabditis elegans Male: Postembryonic Development of Nongonadal Structures. Dev. Biol. *78*, 542–576.

28. Hodgkin, J. (1983). Male Phenotypes and Mating Efficiency in Caenorhabditis Elegans. Genetics *103*, 43–64.

29. Salzberg, Y., Gat, A., and Oren-Suissa, M. (2021). One template, two outcomes: How does the sex-shared nervous system generate sex-specific behaviors? Curr. Top. Dev. Biol. *144*, 245–268.

30. Mori, I. (1999). Genetics of Chemotaxis and Thermotaxis in the Nematode Caenorhabditis elegans. Annu. Rev. Genet., 399–422.

31. Troemel, E.R., Kimmel, B.E., and Bargmann, C.I. (1997). Reprogramming chemotaxis responses: Sensory neurons define olfactory preferences in C. elegans. Cell *91*, 161–169.

32. Chatzigeorgiou, M., Bang, S., Hwang, S.W., and Schafer, W.R. (2013). Tmc-1 encodes a sodium-sensitive channel required for salt chemosensation in C. elegans. Nature *494*, 95–99.

33. Tomioka, M., Adachi, T., Suzuki, H., Kunitomo, H., Schafer, W.R., and Iino, Y. (2006). The Insulin/PI 3-Kinase Pathway Regulates Salt Chemotaxis Learning in Caenorhabditis elegans. Neuron *51*, 613–625.

34. Bretscher, A.J., Kodama-Namba, E., Busch, K.E., Murphy, R.J., Soltesz, Z., Laurent, P., and de Bono, M. (2011). Temperature, oxygen, and salt-sensing neurons in C. elegans are carbon dioxide sensors that control avoidance behavior. Neuron *69*, 1099–1113.

35. Hilliard, M.A., Bargmann, C.I., and Bazzicalupo, P. (2002). C. elegans responds to chemical repellents by integrating sensory inputs from the head and the tail. Curr. Biol. *12*, 730–734.

36. Chalfie, M., and Sulston, J. (1981). Developmental genetics of the mechanosensory neurons of Caenorhabditis elegans. Dev. Biol. *82*, 358–370.

37. Way, J.C., and Chalfie, M. (1989). The mec-3 gene of Caenorhabditis elegans requires its own product for maintained expression and is expressed in three neuronal cell types. Genes and Development *3*, 1823–1833.

38. Pechuk, V., Goldman, G., Salzberg, Y., Chaubey, A.H., Bola, R.A., Hoffman, J.R., Endreson, M.L., Miller, R.M., Reger, N.J., Portman, D.S., et al. (2022). Reprogramming the topology of the nociceptive circuit in C. elegans reshapes sexual behavior. Curr. Biol. *32*, 4372–4385.e7.

39. Setty, H., Salzberg, Y., Karimi, S., Berent-Barzel, E., Krieg, M., and Oren-Suissa, M. (2022). Sexually dimorphic architecture and function of a mechanosensory circuit in C. elegans. Nat. Commun. *13*, 1–15.

40. Edwards, S.L., Charlie, N.K., Milfort, M.C., Brown, B.S., Gravlin, C.N., Knecht, J.E., and Miller, K.G. (2008). A novel molecular solution for ultraviolet light detection in Caenorhabditis elegans. PLoS Biol. 10.1371/journal.pbio.0060198.

41. Iliff, A.J., Wang, C., Ronan, E.A., Hake, A.E., Guo, Y., Li, X., Zhang, X., Zheng, M., Liu, J., Grosh, K., et al. (2021). The nematode C. elegans senses airborne sound. Neuron *109*, 3633–3646.e7.

42. Androwski, R.J., Asad, N., Wood, J.G., Hofer, A., Locke, S., Smith, C.M., Rose, B., and Schroeder, N.E. (2020). Mutually exclusive dendritic arbors in C. elegans neurons share a common architecture and convergent molecular cues. PLoS Genet. *16*, 1–23.

43. Inberg, S., Meledin, A., Kravtsov, V., Iosilevskii, Y., Oren-Suissa, M., and Podbilewicz, B. (2019). Lessons from Worm Dendritic Patterning. Annu. Rev. Neurosci. *42*, 365–383.

44. Oren-Suissa, M., Hall, D.H., Treinin, M., Shemer, G., and Podbilewicz, B. (2010). The fusogen EFF-1 controls sculpting of mechanosensory dendrites. Science *328*, 1285–1288.

45. Smith, C.J., Watson, J.D., Spencer, W.C., O'Brien, T., Cha, B., Albeg, A., Treinin, M., and Miller, D.M. (2010). Time-lapse imaging and cell-specific expression profiling reveal dynamic branching and molecular determinants of a multi-dendritic nociceptor in C. elegans. Dev. Biol. *345*, 18–33.

46. Halevi, S., McKay, J., and Palfreyman, M. (2002). The C.elegans ric-3 gene is required for maturation of nicotinic acetylcholine receptors. EMBO J. 10.1093/emboj/21.5.1012.

47. Yassin, L., Samson, A.O., Halevi, S., Eshel, M., and Treinin, M. (2002). Mutations in the extracellular domain and in the membrane-spanning domains interfere with nicotinic

acetylcholine receptor maturation. Biochemistry *41*, 12329–12335.

48. Cho, Y., Oakland, D.N., Lee, S.A., Schafer, W.R., and Lu, H. (2018). On-chip functional neuroimaging with mechanical stimulation in Caenorhabditis elegans larvae for studying development and neural circuits. Lab Chip *18*, 601–609.

49. Li, W., Kang, L., Piggott, B.J., Feng, Z., and Xu, X.Z.S. (2011). The neural circuits and sensory channels mediating harsh touch sensation in Caenorhabditis elegans. Nat. Commun. *2*, 315.

50. Chatzigeorgiou, M., Yoo, S., Watson, J.D., Lee, W.H., Spencer, W.C., Kindt, K.S., Hwang, S.W., Miller, D.M., Treinin, M., Driscoll, M., et al. (2010). Specific roles for DEG/ENaC and TRP channels in touch and thermosensation in C. elegans nociceptors. Nat. Neurosci. *13*, 861–869.

51. Albeg, A., Smith, C.J., Chatzigeorgiou, M., Feitelson, D.G., Hall, D.H., Schafer, W.R., Miller, D.M., and Treinin, M. (2011). Molecular and Cellular Neuroscience C . elegans multi-dendritic sensory neurons : Morphology and function. Mol. Cell. Neurosci. *46*, 308–317.

52. Tao, L., Porto, D., Li, Z., Fechner, S., Lee, S.A., Goodman, M.B., Xu, X.Z.S., Lu, H., and Shen, K. (2019). Parallel Processing of Two Mechanosensory Modalities by a Single Neuron in C. elegans. Dev. Cell *51*, 1–15.

53. Chen, C.-H., Hsu, H.-W., Chang, Y.-H., and Pan, C.-L. (2019). Adhesive L1CAM-Robo Signaling Aligns Growth Cone F-Actin Dynamics to Promote Axon-Dendrite Fasciculation in C. elegans. Dev. Cell *49*, 490–491.

54. Zou, W., Dong, X., Broederdorf, T.R., Yasuda, R., Chen, B., Zou, W., Dong, X., Broederdorf, T.R., Shen, A., Kramer, D.A., et al. (2018). A dendritic guidance receptor complex brings together distinct actin regulators to drive efficient F-actin assembly and branching. Dev. Cell *45*, 362–375.e3.

55. Sundararajan, L., Smith, C.J., Watson, J.D., Millis, B.A., Tyska, M.J., and Miller, D.M., 3rd (2019). Actin assembly and non-muscle myosin activity drive dendrite retraction in an UNC-6/Netrin dependent self-avoidance response. PLoS Genet. *15*, e1008228.

56. Liu, O.W., and Shen, K. (2011). The transmembrane LRR protein DMA-1 promotes dendrite branching and growth in C. elegans. Nat. Neurosci. *15*, 57–63.

57. Salzberg, Y., Díaz-Balzac, C.A., Ramirez-Suarez, N.J., Attreed, M., Tecle, E., Desbois, M., Kaprielian, Z., and Bülow, H.E. (2013). Skin-derived cues control arborization of sensory dendrites in Caenorhabditis elegans. Cell *155*, 308–320.

58. Dong, X., Liu, O.W., Howell, A.S., and Shen, K. (2013). An Extracellular Adhesion Molecule Complex Patterns Dendritic Branching and Morphogenesis. Cell *155*, 296–307.

59. O'Brien, B.M.J., Palumbos, S.D., Novakovic, M., Shang, X., Sundararajan, L., and Miller, D.M. (2017). Separate transcriptionally regulated pathways specify distinct classes of sister dendrites in a nociceptive neuron. Dev. Biol. *432*, 248–257.

60. Tsalik, E.L., Niacaris, T., Wenick, A.S., Pau, K., Avery, L., and Hobert, O. (2003). LIM homeobox gene-dependent expression of biogenic amine receptors in restricted regions of

the C. elegans nervous system. Dev. Biol. 10.1016/S0012-1606(03)00447-0.

61. Smith, C.J., Watson, J.D., VanHoven, M.K., Colón-Ramos, D.A., and Miller, D.M. (2012). Netrin (UNC-6) mediates dendritic self-avoidance. Nat. Neurosci. *15*, 731–737.

62. Salzberg, Y., Ramirez-Suarez, N.J., and Bülow, H.E. (2014). The proprotein convertase KPC-1/furin controls branching and self-avoidance of sensory dendrites in Caenorhabditis elegans. PLoS Genet. *10*, e1004657.

63. Dong, X., Chiu, H., Park, Y.J., Zou, W., Zou, Y., Özkan, E., Chang, C., and Shen, K. (2016). Precise regulation of the guidance receptor DMA-1 by KPC-1/Furin instructs dendritic branching decisions. Elife *5*, 1–22.

64. Ramirez-Suarez, N.J., Belalcazar, H.M., Rahman, M., Trivedi, M., Tang, L.T.H., and Bülow, H.E. (2023). Convertase-dependent regulation of membrane-tethered and secreted ligands tunes dendrite adhesion. Development *150*, dev201208.

65. Zhu, T., Liang, X., Wang, X.-M., and Shen, K. (2017). Dynein and EFF-1 control dendrite morphology by regulating the localization pattern of SAX-7 in epidermal cells. J. Cell Sci. 10.1242/jcs.201699.

66. Kravtsov, V., Oren-Suissa, M., and Podbilewicz, B. (2017). The fusogen AFF-1 can rejuvenate the regenerative potential of adult dendritic trees by self-fusion. Development *144*, 2364–2374.

67. Brar, H.K., Dey, S., Bhardwaj, S., Pande, D., Singh, P., Dey, S., and Ghosh-Roy, A. (2022). Dendrite regeneration in C. elegans is controlled by the RAC GTPase CED-10 and the RhoGEF TIAM-1. PLoS Genet. *18*, e1010127.

68. Ryan, D.A., Miller, R.M., Lee, K., Neal, S.J., Fagan, K.A., Sengupta, P., and Portman, D.S. (2014). Sex, age, and hunger regulate behavioral prioritization through dynamic modulation of chemoreceptor expression. Curr. Biol. *24*, 2509–2517.

69. Oren-Suissa, M., Bayer, E.A., and Hobert, O. (2016). Sex-specific pruning of neuronal synapses in Caenorhabditis elegans. Nature *533*, 206–211.

70. Barr, M.M., García, L.R., and Portman, D.S. (2018). Sexual Dimorphism and Sex Differences in Caenorhabditis elegans Neuronal Development and Behavior. Genetics *208*, 909–935.

71. Haque, R., Kurien, S.P., Setty, H., Salzberg, Y., Stelzer, G., Litvak, E., Gingold, H., Rechavi, O., and Oren-Suissa, M. (2023). Sex-Specific Developmental Gene Expression Atlas Unveils Dimorphic Gene Networks in C. elegans. bioRxiv, 2023.08.05.552096. 10.1101/2023.08.05.552096.

72. Rahman, M., Ramirez-Suarez, N.J., Diaz-Balzac, C.A., and Bülow, H.E. (2022). Specific N -glycans regulate an extracellular adhesion complex during somatosensory dendrite patterning. EMBO Rep. *23*, 1–17.

73. Zou, W., Shen, A., Dong, X., Tugizova, M., Xiang, Y.K., and Shen, K. (2016). A multi-protein receptor-ligand complex underlies combinatorial dendrite guidance choices in C. elegans. Elife *5*, 1–25.

74. Liang, X., Dong, X., Moerman, D.G., Shen, K., and Wang, X. (2015). Sarcomeres Pattern Proprioceptive Sensory Dendritic Endings through UNC-52/Perlecan in C. elegans. Dev. Cell *33*, 388–400.

75. Singson, A., Hill, K.L., and L'Hernault, S.W. (1999). Sperm competition in the absence of fertilization in Caenorhabditis elegans. Genetics *152*, 201–208.

76. Barr, M.M., and Garcia, L.R. (2006). Male mating behavior. WormBook, 1–11.

77. Liu, K.S., and Sternberg, P.W. (1995). Sensory regulation of male mating behavior in Caenorhabditis elegans. Neuron *14*, 79–89.

78. Chow, K.L., Hall, D.H., and Emmons, S.W. (1995). The mab-21 gene of Caenorhabditis elegans encodes a novel protein required for choice of alternate cell fates. Development *121*, 3615–3626.

79. Yip, Z.C., and Heiman, M.G. (2016). Duplication of a Single Neuron in C . elegans Reveals a Pathway for Dendrite Tiling by Mutual Repulsion. Cell Rep. *15*, 2109–2117.

80. Baird, S.E., Fitch, D.H.A., Kassem, I.A.A., and Emmons, S.W. (1991). Pattern formation in the nematode epidermis: Determination of the arrangement of peripheral sense organs in the C. elegans male tail. Development *113*, 515–526.

81. Mohler, W.A., Shemer, G., Del Campo, J.J., Valansi, C., Opoku-Serebuoh, E., Scranton, V., Assaf, N., White, J.G., and Podbilewicz, B. (2002). The type 1 membrane protein EFF-1 is essential for development cell fusion. Dev. Cell *2*, 355–362.

82. Díaz-Balzac, C.A., Rahman, M., Lázaro-Peña, M.I., Martin Hernandez, L.A., Salzberg, Y., Aguirre-Chen, C., Kaprielian, Z., and Bülow, H.E. (2016). Muscle- and Skin-Derived Cues Jointly Orchestrate Patterning of Somatosensory Dendrites. Curr. Biol. *26*, 2397.

83. Tang, L.T., Diaz-Balzac, C.A., Rahman, M., Ramirez-Suarez, N.J., Salzberg, Y., Lázaro-Peña, M.I., and Bülow, H.E. (2019). TIAM-1/GEF can shape somatosensory dendrites independently of its GEF activity by regulating F-actin localization. Elife *8*, 1–27.

84. Hill, M.H., and Bucknell, P.A. (1987). The Evolution of Fashion: Pattern and Cut from 1066 to 1930 (Batsford).

85. Kim, B., and Emmons, S.W. (2017). Multiple conserved cell adhesion protein interactions mediate neural wiring of a sensory circuit in C. elegans. Elife *6*. 10.7554/eLife.29257.

86. Sakai, N., Iwata, R., Yokoi, S., Butcher, R.A., Clardy, J., and Tomioka, M. (2013). A Sexually Conditioned Switch of Chemosensory Behavior in C . elegans. PloS one *8*, e68676.

87. Zhang, H., Yue, X., Cheng, H., Zhang, X., Cai, Y., Zou, W., Huang, G., Cheng, L., Ye, F., and Kang, L. (2018). OSM-9 and an amiloride-sensitive channel, but not PKD-2, are involved in mechanosensation in C. elegans male ray neurons. Sci. Rep. *8*, 1–8.

88. Koo, P.K., Bian, X., Sherlekar, A.L., Bunkers, M.R., and Lints, R. (2011). The robustness of Caenorhabditis elegans male mating behavior depends on the distributed properties of ray sensory neurons and their output through core and male-specific targets. Journal of Neuroscience *31*, 7497–7510.

89. Wang, X., Kweon, J., Larson, S., and Chen, L. (2005). A role for the C. elegans L1CAM homologue lad-1/sax-7 in maintaining tissue attachment. Dev. Biol. *284*, 273–291.

90. Treinin, M., and Chalfie, M. (1995). A mutated acetylcholine receptor subunit causes neuronal degeneration in C. elegans. Neuron. 10.1016/0896-6273(95)90231-7.

91. Zilkha, N., Sofer, Y., Kashash, Y., and Kimchi, T. (2021). The social network: Neural control of sex differences in reproductive behaviors, motivation, and response to social isolation. Curr. Opin. Neurobiol. *68*, 137–151.

92. Yang, C.F., and Shah, N.M. (2014). Representing sex in the brain, one module at a time. Neuron *82*, 261–278.

93. Barrett, S.C.H., and Hough, J. (2013). Sexual dimorphism in flowering plants. J. Exp. Bot.

94. Hanschen, E.R., Herron, M.D., Wiens, J.J., Nozaki, H., and Michod, R.E. (2018). Multicellularity Drives the Evolution of Sexual Traits. Am. Nat. *192*, E93–E105.

95. Geng, S., De Hoff, P., and Umen, J.G. (2014). Evolution of sexes from an ancestral mating-type specification pathway. PLoS Biol. *12*, e1001904.

96. Umen, J., and Coelho, S. (2019). Algal Sex Determination and the Evolution of Anisogamy. Annu. Rev. Microbiol. *73*, 267–291.

97. Lipinska, A., Cormier, A., Luthringer, R., Peters, A.F., Corre, E., Gachon, C.M.M., Cock, J.M., and Coelho, S.M. (2015). Sexual dimorphism and the evolution of sex-biased gene expression in the brown alga ectocarpus. Mol. Biol. Evol. *32*, 1581–1597.

98. Alshammari, T.K. (2021). Sexual dimorphism in pre-clinical studies of depression. Prog. Neuropsychopharmacol. Biol. Psychiatry *105*, 110120.

99. Dennison, J.L., Ricciardi, N.R., Lohse, I., Volmar, C.-H., and Wahlestedt, C. (2021). Sexual dimorphism in the 3xTg-AD mouse model and its impact on pre-clinical research. J. Alzheimers. Dis. *80*, 41–52.

100. Davies, W. (2014). Sex differences in attention Deficit Hyperactivity Disorder: candidate genetic and endocrine mechanisms. Front. Neuroendocrinol. *35*, 331–346.

101. Donald, S., Humby, T., Fyfe, I., Segonds-Pichon, A., Walker, S.A., Andrews, S.R., Coadwell, W.J., Emson, P., Wilkinson, L.S., and Welch, H.C.E. (2008). P-Rex2 regulates Purkinje cell dendrite morphology and motor coordination. Proc. Natl. Acad. Sci. U. S. A. *105*, 4483–4488.

102. Yoon, H., Enquist, L.W., and Dulac, C. (2005). Olfactory inputs to hypothalamic neurons controlling reproduction and fertility. Cell *123*, 669–682.

103. Jois, S., Chan, Y.B., Fernandez, M.P., Pujari, N., Janz, L.J., Parker, S., and Leung, A.K.W. (2022). Sexually dimorphic peripheral sensory neurons regulate copulation duration and persistence in male Drosophila. Sci. Rep. *12*, 1–12.

104. Belote, J.M., and Baker, B.S. (1987). Sexual behavior: its genetic control during development and adulthood in Drosophila melanogaster. Proc. Natl. Acad. Sci. U. S. A. *84*, 8026–8030.

105. Husson, S.J., Costa, W.S., Wabnig, S., Stirman, J.N., Watson, J.D., Spencer, W.C., Akerboom, J., Looger, L.L., Treinin, M., Miller, D.M., et al. (2012). Optogenetic Analysis of a Nociceptor Neuron and Network Reveals Ion Channels Acting Downstream of Primary Sensors. Curr. Biol. *22*, 743–752.

106. Muirhead, C.S., and Srinivasan, J. (2020). Small molecule signals mediate social behaviors in C . elegans. Journal of neurogenetics *34*, 395–403.

107. Luo, J., Bainbridge, C., Miller, R.M., Barrios, A., and Portman, D.S. (2024). C. elegans males optimize mate-preference decisions via sex-specific responses to multimodal sensory cues. Curr. Biol. *34*, 1309–1323.e4.

108. Brugman, K.I., Susoy, V., Whittaker, A.J., Palma, W., Nava, S., Samuel, A.D.T., and Sternberg, P.W. (2022). PEZO-1 and TRP-4 mechanosensors are involved in mating behavior in Caenorhabditis elegans Significance Statement : 1–12.

109. Barrios, A., Nurrish, S., and Emmons, S.W. (2008). Sensory Regulation of C. elegans Male Mate-Searching Behavior. Curr. Biol. *18*, 1865–1871.

110. Wexler, L.R., Miller, R.M., and Portman, D.S. (2020). Article C . elegans Males Integrate Food Signals and Biological Sex to Modulate State-Dependent Chemosensation and Behavioral Prioritization ll Article C . elegans Males Integrate Food Signals and Biological Sex to Modulate State-Dependent Chemosensation. Curr. Biol. *30*, 2695–2706.e4.

111. Susoy, V., Hung, W., Witvliet, D., Whitener, J.E., Wu, M., Park, C.F., Graham, B.J., Zhen, M., Venkatachalam, V., and Samuel, A.D.T. (2021). Natural sensory context drives diverse brain-wide activity during C. elegans mating. Cell *184*, 5122–5137.e17.

112. Tao, L., Coakley, S., Shi, R., and Shen, K. (2022). Dendrites use mechanosensitive channels to proofread ligand-mediated neurite extension during morphogenesis. Dev. Cell *57*, 1615–1629.e3.

113. Cohen, E., Yemini, E., Schafer, W., Feitelson, D.G., and Treinin, M. (2012). Locomotion analysis identifies roles of mechanosensory neurons in governing locomotion dynamics of C. elegans. J. Exp. Biol. *215*, 3639–3648.

114. Jia, L., and Emmons, S.W. (2006). Genes that control ray sensory neuron axon development in the Caenorhabditis elegans male. Genetics *173*, 1241–1258.

Figure legends

Figure 1 WT male PVD development shows post-larval sexual dimorphism

(A,B) Hermaphrodite PVD development in L4 and adult, respectively. PVD branch orders are marked yellow in panel B. Anterior is left, ventral down.

(C-F) Male PVD development through larval stages L3, L4 and adult; white numbers and arrows note tail ray pairs; PVD branch orders are marked yellow. Scale bar is 50 μm.

(G) Analysis of PVD branches. *t* test, Holm-Šídák multiple comparison correction. Black bars show mean, error bars show ±SD. $p<0.05$ (*), $p<0.01$ (**), $p<0.001$ (***); $p<0.0001$ (****).

(H) Ectopic branches around the cell body region in 1-day adult animals, normalized per 100 μm of the primary branch for the different branching orders; n=16 (6 PVDL,10 PVDR) hermaphrodite and n=12 (7 PVDL, 5 PVDR) males. *t* test, Holm-Šídák multiple comparison correction. Black bars show mean, error bars show ±SD (except male ectopic tertiaries and ectopic quaternaries, showing +SD).

(I) Cartoon depiction of the male tail organ; lateral view contains a tracing of the neuron in panel D: projection of three-dimensional trace, branch orders annotated blue (1°), purple (2°), red (3°), cyan (4°) and yellow (5° and 6° order ectopics); scale bar is 50 μm; PVD branch orders are marked in black following panel F. Scale bar is 50 μm.

(J) Percentage of animals with visible PVD signal in the individual rays 1-9 on the left and right sides. Young adults: two days from egg; n=28 animals; One day adults: three days from embryo, n=10; Two-day adults: four days from egg, n=21; three-day adults: five days from egg, n=11 animals. Not all rays were visible in all animals; at least five animals are analyzed in every ray. Rays 8-9, which are sometimes fused, are joined for consistency, and represent a signal in either 8,9, or both. A cartoon depiction of a dorsal tail view is presented for orientation. Animals in panels A-F and J carry a *him-5(e1490)* background to increase male percentage.

Figure 2 Mutants affecting hermaphrodite PVD morphology show similar male phenotypes

(A) Male one-day adult WT PVD (*ser2prom3::*GFP*)*. White arrows mark tail rays showing a PVD signal.

(B**)** Male one-day adult *eff-1(ok1021);him-5(e1490);ser2prom3::*GFP PVD, white arrows mark (empty) residual rays. yellow arrows point to examples of characteristic altered hyperbranched structure.

(C) Male one-day adult *mec-3(e1338);him-5(e1490);ser2prom3::*GFP PVD*,* orange arrowhead marks the posterior-most branch.

(D) Male one-day adult *sax-7(dz156);pF49H12.4::*GFP*,* yellow arrows point to examples of characteristic altered structure, orange arrowhead marks the posterior-most branch.

(E) Male one-day adult *mnr-1(dz175);pF49H12.4::*GFP, yellow arrows point to examples of characteristic altered structure, orange arrowhead marks the posterior-most branch.

(F) Male one-day adult *dma-1(tm5159);pF49H12.4::*GFP*,* yellow arrow points to characteristic altered structure, orange arrowhead marks the posterior-most branch.

(G**)** *mab-20(bx61ts);him-5(e1490);ser2prom3::*GFP 1-2-day adult at a semi-restrictive 22°C temperature, yellow arrow marks a characteristic 'fusion' joining rays 3 and 4.

(H) PVD genetic ablation *ser2prom3::deg-1(u662);him-5(e1490);ser2prom3::*Kaede two-day adult showing signal remnant (arrow) next to the PVD soma, possibly PDE, with ventral truncated axon-like process. (*him-5(e1490)* background). Scale bar is 50 µm.

(I) Quantification of PVD entry into the tail rays in different mutant backgrounds and ages; all animals assayed express the integrated *ser2prom3*::GFP PVD marker and are *him-5(e1490*), with the exception of *deg-3(u662)* genetic ablation which utilizes a Kaede fluorescent marker and *sax-7(dz156), mnr-1 (dz175)* and *dma-1(tm5159)* which express an integrated *pF49H12.4*::GFP PVD marker and are without *him-5*; YA: young adult; A1d, A1.5d, A2d, A3d, A4d: 1, 1.5, 2, 3 and 4-day adult, respectively. Day 1 adult = L4 + 1 day. n =15, 28, 10, 21, 11, 13, 11,10, 5, 10, 15, 12,13, 18, respectively. For *mab-20(bx61ts)*, one day from L4 at room

temperature is comparable with to L4 + 28 h at 20°C and as such marked 1.5 day adult. One-way ANOVA, Šídák multiple comparison correction. Black bars show mean, error bars show ±SD. $p<0.05$ (*), $p<0.01$ (**), $p<0.001$ (***); $p<0.0001$ (****).

Figure 3 RnB neuron and *sax-7*::GFP signal appear in rays prior to PVD extension

(A) L4 stage GFP signal of RnB marker *pkd-2*::GFP and PVD marker *pF49H12.4*::mCherry. RnB signal was observed in 54/54 nascent tail rays (excluding ray 6; yellow arrow), with 0/54 showing PVD signal.

(B) Respective DIC image of A.

(C,D) Merged images of PVD marker *pF49H12.4*::mCherry (pseudocolored cyan) and RnB marker *pkd-2*::GFP (pseudocolored magenta; see also Video S4) over DIC (gray) during late L4 (lateral view) and adult (dorsal view), respectively. RnB signal was observed in 92/92 adult tail rays (excluding ray 6), with PVD signal in 67/92 (of which nine cases of partial entry). Red arrows point to tail rays; yellow arrows indicate ray pair six, white arrowheads point to the pre-anal ganglion region.

(E,G) Male tail with *sax-7* reporter during development. Signal observed in 43/43 nascent (L4) rays.

(I) Adult lateral view of merged *sax-7* reporter with PVD marker, 'inverted' pseudo-colors are used for clarity. 113/113 one-day adult rays observed with SAX-7 signal, of which 79/113 with PVD signal.

(F, H, J) Matching DIC images to E,G,I, respectively. Red arrows point to tail rays. Scale bar is 50 µm.

Figure 4 Mating behavior is impaired under PVD genetic ablation

(A) Cartoon of mating steps. Male presented in purple, hermaphrodite in green.

(B-D) Hermaphrodite recognition, turning and vulva recognition, respectively, in WT and *ser2prom3*::*deg-3(u662)* animals where PVD undergoes early degeneration. B: n=18 WT, n=18 *ser2prom3*::*deg-3(u662)*; C: n=16 WT, 18 *ser2prom3*::*deg-3(u662)*; D: n=18 WT, 18 *ser2prom3*::*deg-3(u662)*. Perfect turn is defined as a turn completed successfully without the male tail losing contact with the hermaphrodite. *t* test, black bars show mean, error bars show ±SD. $p<0.05$ (*), $p<0.01$ (**), $p<0.0001$ (****).

Figure 5 Proposed model for PVD male-specific morphology and role in *C. elegans*

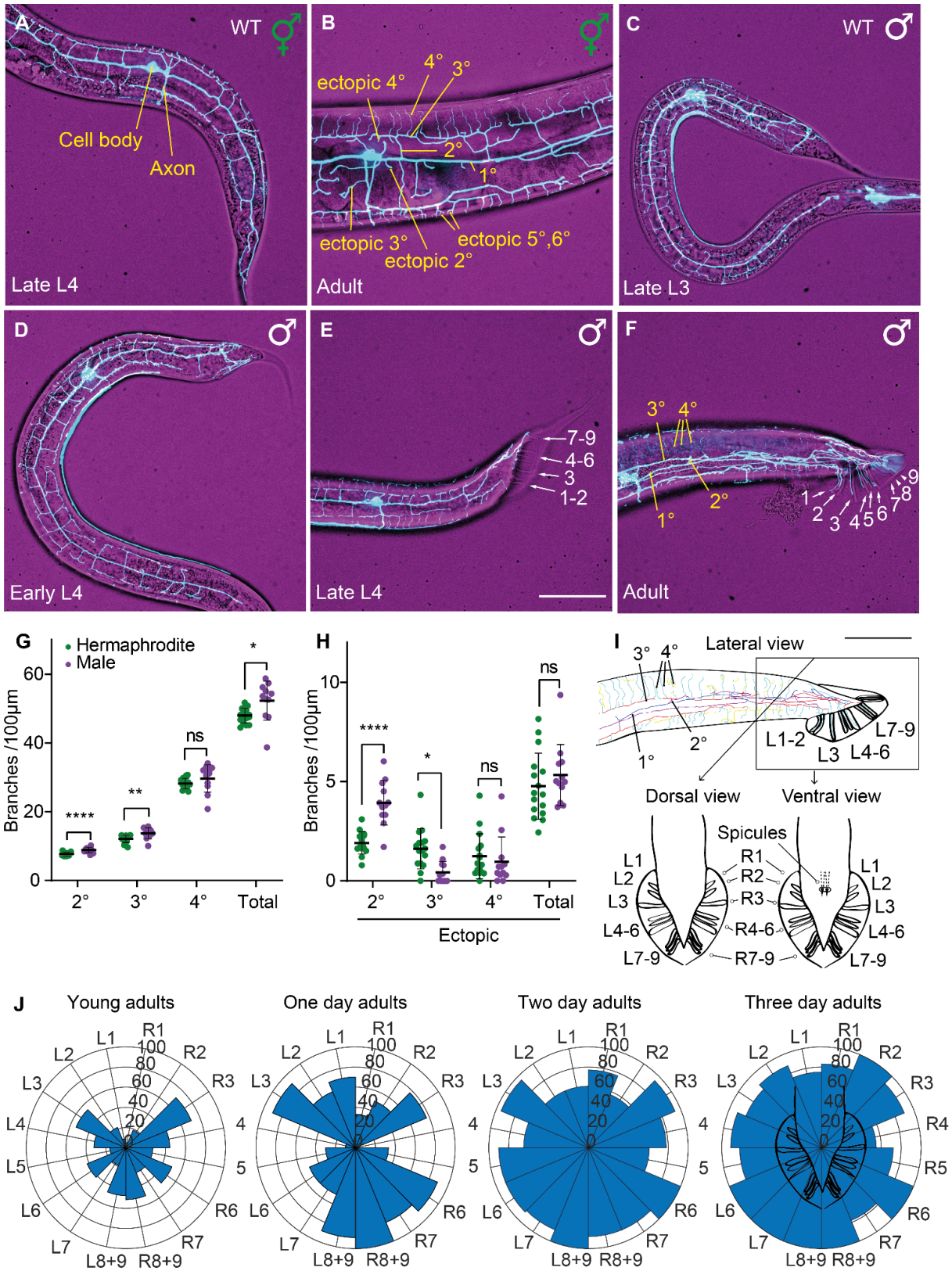

Figure 1 WT male PVD development shows post-larval sexual dimorphism

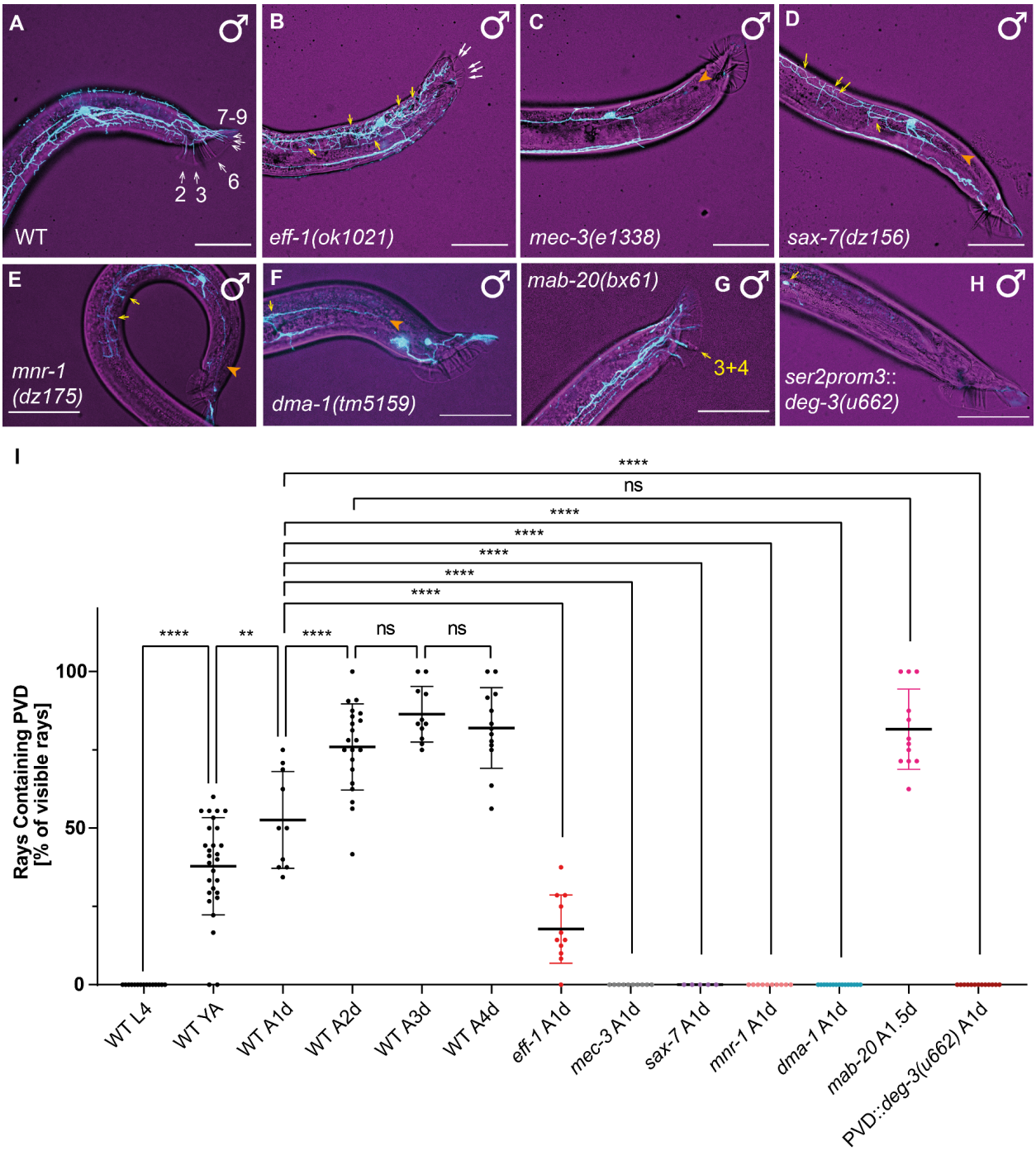

Figure 2 Mutants affecting hermaphrodite PVD morphology show similar male phenotypes

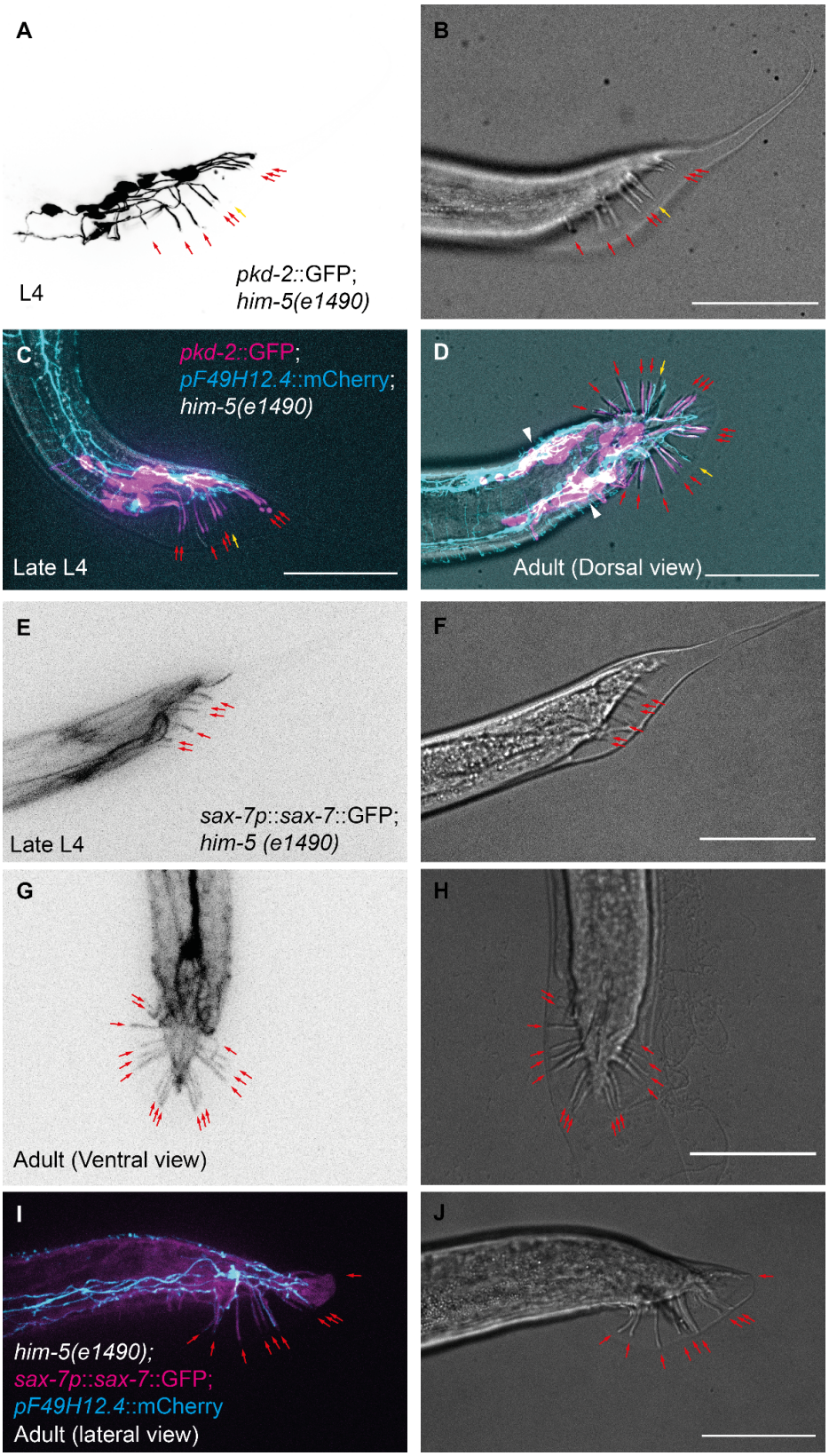

Figure 3 RnB neuron and *sax-7*::GFP signal appear in rays prior to PVD extension

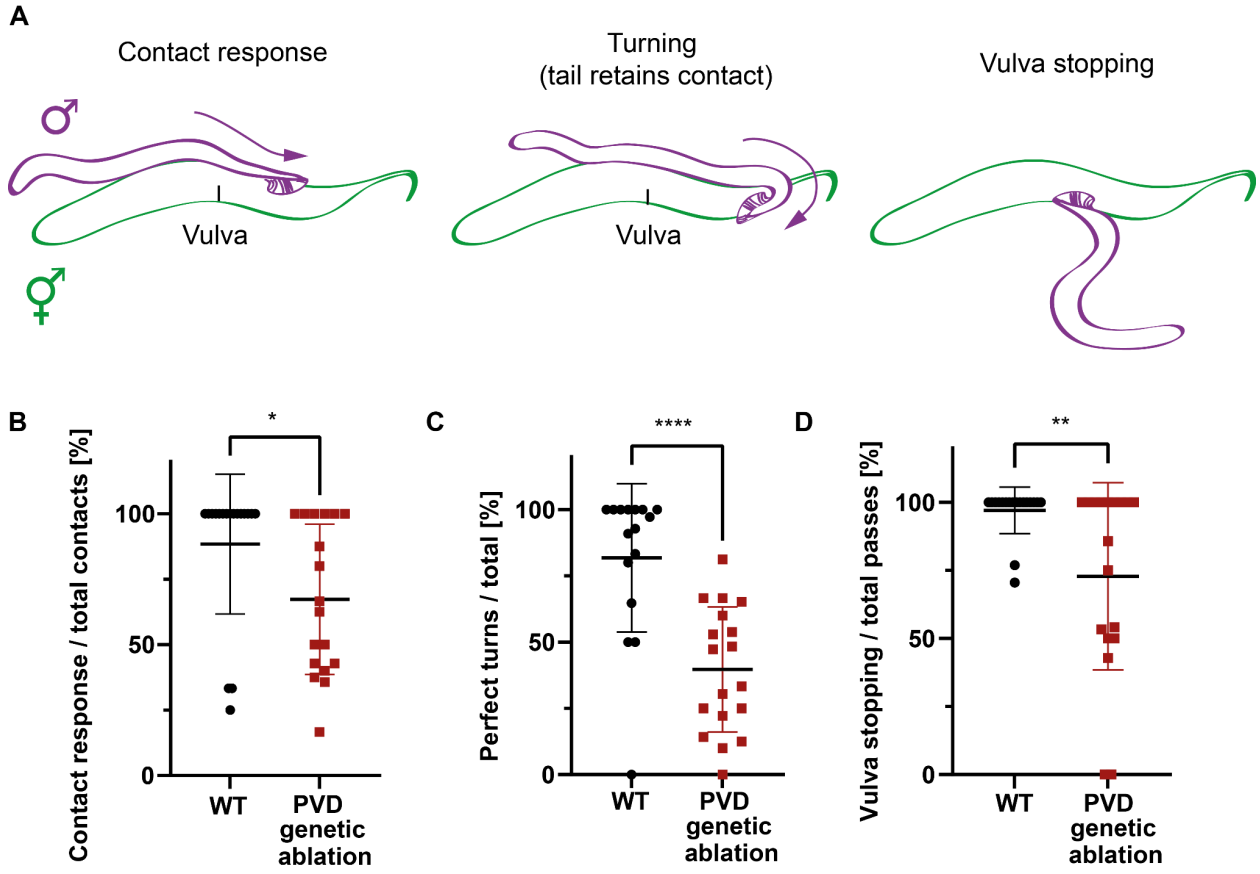

Figure 4 Mating behavior is impaired under PVD genetic ablation

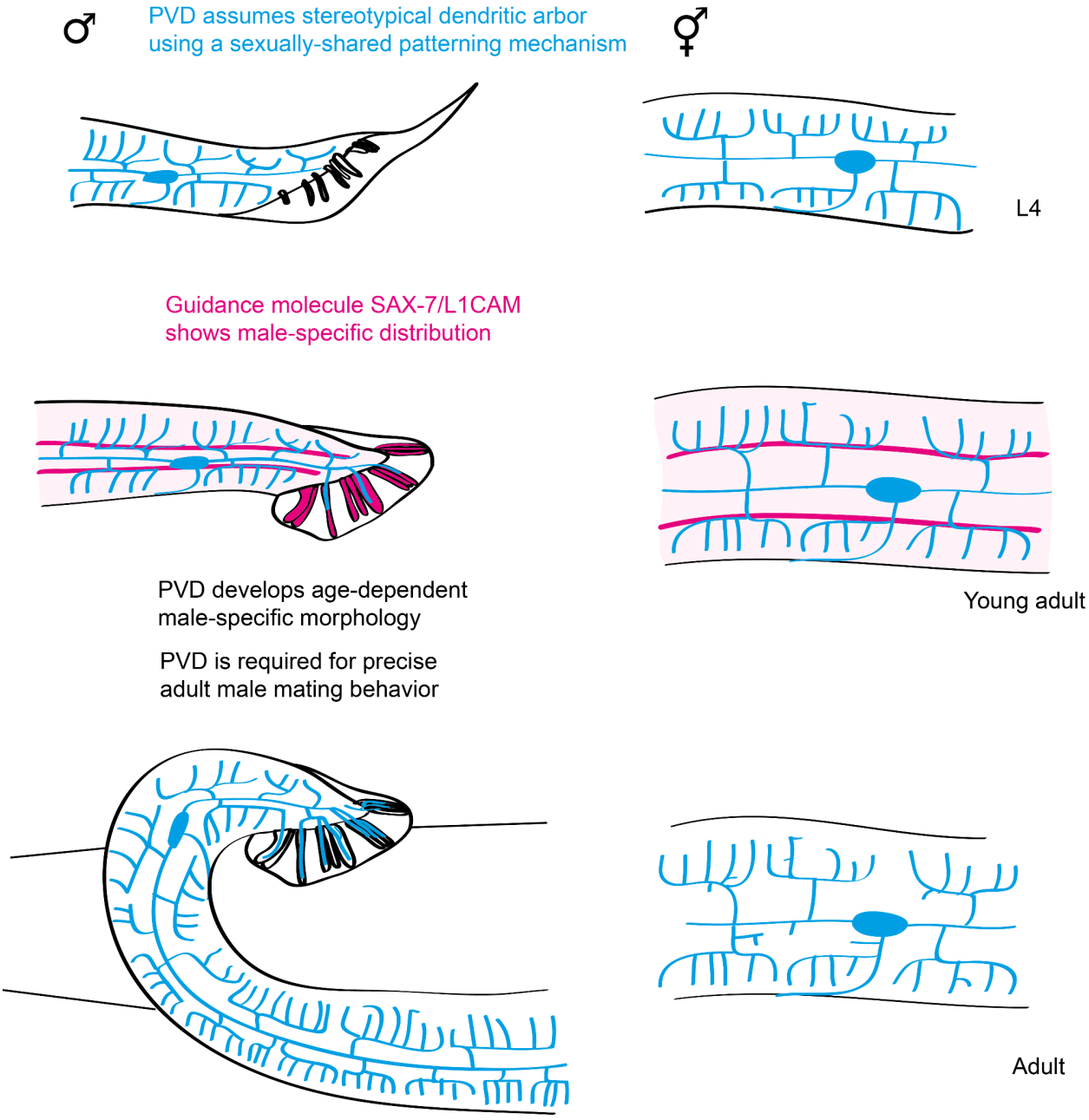

Figure 5 Proposed model for PVD male-specific morphology and role in *C. elegans*